

# Simulations of Shor's Algorithm using Matrix Product States

D. S. Wang,<sup>\*</sup> C. D. Hill,<sup>†</sup> and L. C. L. Hollenberg<sup>‡</sup>  
*Centre for Quantum Computation and Communication Technology,  
 School of Physics, The University of Melbourne, Parkville, Victoria 3010, Australia*

We show that under the matrix product state formalism the states produced in Shor's algorithm can be represented using  $O(\max(4lr^2, 2^{2l}))$  space, where  $l$  is the number of bits in the number to factorise, and  $r$  is the order and the solution to the related order-finding problem. The reduction in space compared to an amplitude formalism approach is significant, allowing simulations as large as 42 qubits to be run on a single processor with 32GB RAM. This approach is readily adapted to a distributed memory environment, and we have simulated a 45 qubit case using 8 cores with 16GB RAM in approximately one hour.

PACS numbers: 03.67.Ac, 03.67.Lx

## I. INTRODUCTION

Running large-scale quantum algorithms on a quantum computer is still a distant goal. The qubit [1] is a two-level system which can be in superpositions of both states, and is the fundamental unit of information for quantum computation. Not only is creating large numbers of qubits with precise control difficult, so too is preserving the delicate entanglement. Thus, classical simulation is essential to study the tolerance of quantum algorithms against qubit decoherence and control errors.

Shor's algorithm for prime number factorisation [2, 3] is a well known quantum algorithm, and has been simulated extensively in the amplitude formalism [4–8]. The computational resources grow exponentially with system size and the simulation results are easily verified, making it an ideal test candidate. Amplitude formalism simulators have simulated systems with as many as 42 qubits on massive supercomputers [7, 8], using highly parallelised software. These calculations represent the current limit using the amplitude formalism.

Here we consider a different approach to classical quantum algorithm simulation. The *matrix product state* (MPS) formalism [9] is a specialised form of tensor network where the interacting bodies are confined to one dimension. Briefly, each quantum state is represented as a product of matrices. The matrix dimensions depend on the entanglement in the system, and exceptional cases may lead to an efficient simulation. Fortunately for quantum computing, this is not the case for Shor's algorithm. Nonetheless, MPS can be useful for circuit simulation.

In this paper, we shall show that the space requirements for running Shor's algorithm using a MPS simulator is  $O(\max(4lr^2, 2^{2l}))$ , where  $l$  is the number of bits in the number  $N$  to factorise, and  $r$  is the order of the related order-finding problem. The space reduction com-

pared to the  $O(2^{3l})$  of amplitude formalism simulators allows us to simulate a 42 qubit case on a single processor with 32GB RAM in a matter of hours. We discuss optimisation techniques that arise from circuit. We also reason that MPS simulators are well suited to parallelisation, and demonstrate near ideal scaling using MPI. Our largest simulation instance consisted of 45 qubits, using 8 processor cores with 16GB RAM in approximately one hour (real time).

This paper is organised as follows. Section II is a review of Shor's algorithm. Section III is a review of MPS. Section IV analyses the space performance of Shor's algorithm when stored as a MPS. Section V describes our implementation in detail, and tabulates single process benchmarks. Section VI discusses a multi-processor implementation, and benchmarks indicate good scaling behaviour.

## II. REVIEW OF SHOR'S ALGORITHM

We shall give a brief review of Shor's algorithm [2, 3]. Given an  $l$ -bit number  $N = p \times q$ , where the integers  $p$  and  $q$  are co-prime, the task is to determine the factors  $p$  and  $q$ . This is canonically achieved by reduction to a related *order-finding* problem: for a chosen integer  $x$ , where  $1 < x < N$ , find the *order*  $r$  of  $x$  modulo  $N$ . The order  $r$  is the smallest positive integer satisfying

$$x^r \equiv 1 \pmod{N}. \quad (1)$$

It can be shown that for even valued  $r$  and  $x^{r/2} \neq -1 \pmod{N}$ , one can find the factors of  $N$  by computing the greatest common denominator  $\gcd(x^{r/2} \pm 1, N)$ . This can be performed efficiently by Euclid's algorithm. The quantum order-finding circuit (Fig 1) that lies at the heart of Shor's algorithm allows a quantum computer to *efficiently* determine the order  $r$ , using qubits and circuitry growing only polynomially with  $l$ . It consists of  $3l$  qubits divided into two registers: the upper  $2l$  qubits are initialised in  $|0\rangle$ , and the remaining  $l$  qubits are initialised in  $|1\rangle$ . In the figure,  $H = (\sigma_x + \sigma_z)/\sqrt{2}$  is the *Hadamard*

<sup>\*</sup> dswang@physics.unimelb.edu.au

<sup>†</sup> cdhill@unimelb.edu.au

<sup>‡</sup> lloydch@unimelb.edu.au

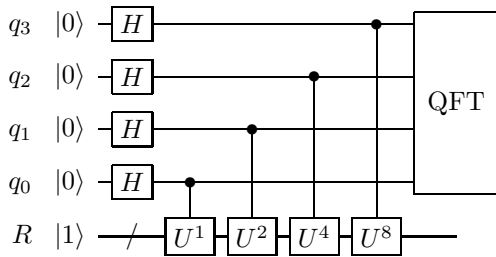


FIG. 1. Schematic of the order-finding circuit which efficiently determines the order  $r$ . To factorise an  $l$ -bit number  $N$ , one uses an upper register with  $2l$  qubits, a lower register  $R$  with  $l$  qubits, and  $U|a\rangle = |ax \bmod N\rangle$  for some integer  $1 < x < N$ . QFT is the quantum Fourier transform.

operation, where  $\sigma_x$  and  $\sigma_z$  are the Pauli matrices, the unitary  $U$  performs

$$U|a\rangle = |ax \bmod N\rangle, \quad (2)$$

and QFT denotes the *quantum Fourier transform* [10]. Neglecting normalisation constants, one can show that the state created after the controlled- $U$ s have been applied is

$$|\psi\rangle = \sum_{i=0}^{2^{2l}-1} |i\rangle |x^i \bmod N\rangle. \quad (3)$$

We shall always suppress the Kronecker or tensor product between two kets (i.e.  $|a\rangle|b\rangle \equiv |a\rangle \otimes |b\rangle$ ). Substituting in Eqn 1 allows one to rewrite this as

$$|\psi\rangle = \sum_{i=0}^{r-1} \left( \sum_{j=0}^{r-1} |jr+i\rangle \right) |x^i \bmod N\rangle. \quad (4)$$

After applying all of the controlled- $U$ s, one can measure and discard the lower register, leaving a system containing only  $2l$  qubits. The QFT produces a probability distribution in the upper register with high probability densities in states around integer multiples of  $2^{2l}/r$ . The results of a few measurements from this probability distribution can be classically processed into  $r$  via the continued fractions algorithm. Since it is possible to construct circuits to efficiently perform all powers of  $U$  [11, 12] and the QFT [10], it is therefore possible for a quantum computer to efficiently determine the order  $r$  and hence factorise large numbers.

### III. REVIEW OF MATRIX PRODUCT STATES

Here we briefly review the MPS formalism [9]. The reader may be familiar with *amplitude formalism* state vector simulators, where one stores the state as a collection of complex coefficient-index pairs. Typically this is implemented as a complex number along a contiguous array. This approach requires space governed only

by the size of the system, regardless of the state stored. The MPS formalism is a different way to store the state, where the space required grows as the state becomes entangled, by using the ability to write a general quantum state  $|\psi\rangle$  as

$$|\psi\rangle = \sum_{abc\dots} (A_a B_b C_c \dots) |a\rangle |b\rangle |c\rangle \dots \quad (5)$$

Here  $|a\rangle$ ,  $|b\rangle$ ,  $|c\rangle$ , etc. are the bases of the subsystems of the state, and  $A_a$ ,  $B_b$ ,  $C_c$ , etc. are matrices associated with the respective subsystems. That is, the amplitude  $\alpha_{abc\dots}$  of the state is stored as the matrix product  $A_a B_b C_c \dots$ . The indices  $a$ ,  $b$ ,  $c$ , etc. span the dimensions of their respective subsystems (e.g. for a qubit, the index can be zero or one), allowing for straightforward generalisations to  $d$ -level subsystems (i.e. *qudits*). Indeed, any two or more neighbouring qudits in a MPS—that is, their matrices are adjacent in the product—can be combined into a single higher-dimensional qudit simply by the evaluating the different matrix products and redefining the subsystems (e.g.  $D_d \equiv D_{ab} \equiv A_a B_b$ ).

A single-qudit gate  $U_1$  is applied by mapping  $U_1$  between the corresponding elements in the matrices associated with that qudit only. Many-qudit gates (assuming all involved qudits form a contiguous sequence) can be applied by first contracting those qudits together, thus forming a single qudit, and then applying the equivalent single-qudit gate on the combined system. Swap gates can be used to rearrange qudits amongst one another when interacting initially distant qudits. Finally, one can separate the composite system back into the original partitions, or as desired, by applying a matrix decomposition algorithm on an specifically arranged matrix:

$$\begin{bmatrix} D_{00} & D_{01} & \dots & D_{0j} \\ D_{10} & D_{11} & \dots & D_{1j} \\ \vdots & \vdots & \ddots & \vdots \\ D_{i0} & D_{i1} & \dots & D_{ij} \end{bmatrix} = \begin{bmatrix} A_0 \\ A_1 \\ \vdots \\ A_i \end{bmatrix} [B_0 \ B_1 \ \dots \ B_j]. \quad (6)$$

The left-hand side shows the arrangement of the matrices  $D_{ab}$ , where  $0 \leq a \leq i$  and  $0 \leq b \leq j$ , of the composite qudit within a single  $m \times n$  matrix, for decomposition into a left  $(i+1)$ -dimensional qudit and a right  $(j+1)$ -dimensional qudit. A matrix decomposition algorithm returns the two right-hand side matrices (or something similar), which have dimensions  $m \times k$  and  $k \times n$ , where  $k$  is ideally the *rank* of the left-hand side matrix (the number of linearly independent rows or columns). After the decomposition, one can readily extract the matrices  $A_a$  and  $B_b$ . Rank-revealing decompositions such as the *singular value decomposition* (SVD) and the *pivoted QR decomposition* (RRQRF), although not strictly necessary, are beneficial as they minimise  $k$  and, hence, the required storage space.

Note that, due to numerical imprecision, the rank is normally understood to be the number of eigenvalues above a given threshold returned by the SVD, and one

can introduce a form of approximation by raising the cut-off value. MPS was developed as an efficient method for simulating systems where the number of non-trivial eigenvalues is limited. However, for the controlled- $U$  gates in the order-finding circuit, the eigenvalues are either clearly zero or non-zero, thus increasing the cut-off value does not provide any benefit (without invalidating the results).

#### IV. ORDER-FINDING CIRCUIT SPACE ANALYSIS

Amplitude formalism state vector simulators are severely limited by the number of qubits in the circuit. In the case of the order-finding circuit, the most resource intensive state under the amplitude formalism is the state as one applies the final controlled- $U$  operation (Eqn 4), requiring  $O(2^{3l})$  space for a standard implementation, and  $O(2^{2l})$  space for one using sparse storage.

We now show that the state in Eqn 4 can be stored much more economically by using the MPS formalism. We wish to first divide this state into two qudits: a left-hand side ket which is the contraction of the upper  $2l$  control qubits, and a right-hand side ket for lower  $l$  qubits. A general state with this division can be written as

$$|\psi\rangle = \sum_{a=0}^{2^{2l}-1} \sum_{b=0}^{2^l-1} A_a B_b |a\rangle |b\rangle. \quad (7)$$

Here  $A_a$  and  $B_b$  are complex row and column vectors respectively, so that the product  $A_a B_b$  is a scalar. We note that in Eqn 4, the summation index  $i$  spans  $r$  values only, corresponding to the  $r$  unique values generated by  $x^i \bmod N$ . From this comparison, one concludes that there are only  $r$  non-trivial  $B_b$  matrices in Eqn 7. For linear independence, the  $B_b$  matrices must contain at least  $r$  rows. The  $A_a$  matrices must possess as many columns as  $B_b$  does rows to satisfy the matrix product. It follows that for this particular decomposition, the state can be expressed with  $O(2^{2l} [1 \times r] + r [r \times 1])$  space.

One can further decompose the left-hand side ket down to individual control qubits. Each of the  $2l$  control qubits' two bases can be represented by matrices no greater than  $r \times r$ . This is easily seen from the structure of the order-finding circuit; the control qubits only interact with the lower register, and *not* with one another. Using this decomposition, Eqn 4 can be represented using  $O(2l \cdot 2 [r \times r])$  space.

To illustrate the above analysis, see Table I. Here we have graphed the ranks across the MPS after each controlled- $U$  gate is applied for the case  $N = 65$ ,  $x = 2$ , and  $r = 12$ . We shall describe our implementation in detail in Section V. For now, it suffices to know that adjacent pairs of numbers define the dimensions of the intermediate matrix. One can see that no matrix exceeds dimensions  $r \times r$ .

Increasing Unitary Order								
$U^1$	1	...	1	1	1	1	2	1
$U^2$	1	...	1	1	1	1	2	4
$U^4$	1	...	1	1	1	2	4	8
$U^8$	1	...	1	1	2	4	8	12
$U^{16}$	1	...	1	2	4	8	12	12
$U^{8192}$	1	2	4	8	12	12	...	<u>12</u>

TABLE I. The ranks across the MPS after completing the order-finding circuit up to and including the indicated controlled-unitary for  $N = 65$ ,  $x = 2$ ,  $l = 7$ . Increasing time flows down the table. Adjacent pairs of numbers define the dimensions of the intermediate matrix. The lower register is stored at the rightmost end, so that the second last number in each row is also equal to the number of non-trivial states in the lower register. The underlined value is the order  $r = 12$ . The final order of qubits is  $q_0, q_1, \dots, q_{13}$ .

Decreasing Unitary Order								
$U^{8192}$	1	...	1	1	1	1	2	1
$U^{4096}$	1	...	1	1	1	1	2	3
$U^{2048}$	1	...	1	1	1	2	3	3
$U^4$	1	2	3	3	...	3	3	3
$U^2$	1	2	3	3	...	3	3	6
$U^1$	1	2	3	3	...	3	6	<u>12</u>

TABLE II. Applying controlled-unitaries in decreasing powers of two lead to equal or lower ranks across the MPS (cf. Table I), thus improves both space and time performance. The final order of qubits is  $q_{13}, q_{12}, \dots, q_0$ .

The remainder of the circuit can be completed by first measuring and discarding the lower register, leaving behind a  $2l$  qubit system. All of the control qubits can then be contracted to a single qudit. At this point, the MPS representation becomes equivalent to the amplitude formalism representation, thus it requires  $O(2^{2l})$  space. Therefore, the entire order-finding circuit can be completed using  $O(\max(4lr^2, 2^{2l}))$  space. Further space reduction is possible by using sparse matrices—after reading Section V, it should become obvious that the space required before the QFT is  $O(lr)$ .

Note that the of value  $r$  will arise naturally as the simulation is run. It is interesting to observe that in  $r < \log_2 N$  cases, one can efficiently simulate Shor's algorithm by using the semi-classical QFT [13, 14]. However, it is exceedingly rare to choose an  $x$  with  $r < \log_2 N$  [15]. Furthermore, for the case  $x = N - 1$ , it is easy to check that  $r = 2$ , but the algorithm does not return any non-trivial factors.

#### V. IMPLEMENTATION AND BENCHMARKS

We now describe the details of our simulations and present our benchmarks. Preliminary processing steps

required before the order-finding circuit available elsewhere (e.g. see [1]) and will not be repeated here. We shall divide the circuit into three distinct steps: (1) the application of the controlled- $U$  gates; (2) the measurement of the lower register; and, (3) the final quantum Fourier transform.

The circuit consists of  $2l$  control qubits, labelled  $q_i$ ,  $0 \leq i < 2l$ , such that the qubit  $q_i$  controls the gate  $U^{2^i}$ . The remaining  $l$  qubits form the lower register  $R$ . They are always contracted into a single  $2^l$ -dimensional qudit (technically, the circuit also works with a single  $N$ -dimensional qudit). Following our space analysis, we choose only to store the non-trivial matrices of  $R$  (at most  $r$ ), and furthermore, we choose to always keep it at the rightmost end of the product, so that these matrices are always column vectors, each containing at most  $r$  rows.

The state is initialised in  $|0\rangle|1\rangle$ . The  $H$  gates may be applied immediately, or combined into the following controlled- $U$  gates. We have opted to implement the latter. In both cases, all of the matrices representing the state are, at present, simply scalars—either 0, 1, or  $1/\sqrt{2}$ —and thus the internal ordering amongst qubits and qudits is negligible. Note, however, that for a general entangled state, the ordering is of critical importance.

### A. The Controlled- $U$ Gates

In order to apply the controlled- $U^{2^i}$  gate, we first shift the control qubit  $q_i$  directly to the left of lower register  $R$ . Since  $q_i$  is in a product state, or more correctly, its matrices are currently scalars, one can commute it through the matrix product with ease, and resize it (i.e. multiplying it by an appropriately sized square identity matrix) to retain a well-formed MPS.

Now one can contract  $q_i$  with  $R$ , and subsequently apply the controlled operation. Let this combined system have matrices denoted by  $D_{ab}$ , where  $a \in \{0, 1\}$  and  $b$  are the non-trivial states of  $R$ . Then, in order to separate the system into two partitions, with  $q_i$  on the left and  $R$  on the right, one arranges the matrices  $D_{ab}$  into a single matrix as shown on the left-hand side of Eqn 6. In practice, instead of performing each of these steps independently, one can perform the contraction, apply the controlled- $U$  gate, and arrange the  $D_{ab}$  matrices in a single swift blow for efficiency. Additionally, the  $H$  operation on  $q_i$ , which simply takes the state from  $|0\rangle$  to  $(|0\rangle + |1\rangle)/\sqrt{2}$ , is also readily combined into the above steps.

A matrix decomposition algorithm takes the matrix on the left-hand side of Eqn 6 and produces the two matrices on the right-hand side. These contain the new matrices associated with the states of  $q_i$  and  $R$ . Note that the decomposition is not unique. As mentioned earlier, the intermediate dimension is minimised by using a rank-revealing decomposition, and is at best the rank  $k$  of the left-hand side matrix. However, in this case, we know  $k$  is exactly the number of non-trivial states of  $R$ . Furthermore, we have arranged the matrix such that

there are  $k$  columns (we can think of this as pivoting the trivial columns to the end of the matrix). For the sake of speed yet still maintaining the space performance of MPS, whenever one suspects an  $m \times n$  matrix  $A$  having rank  $k \approx \min(m, n)$ , as is the case here, one can use the trivially simple decomposition:

$$A_{m \times n} = \begin{cases} A_{m \times n} I_{n \times n}, & m \geq n \\ I_{m \times m} A_{m \times n}, & m < n \end{cases}. \quad (8)$$

The above discusses how a single controlled- $U$  gate is implemented. The circuit consists of  $2l$  such gates, which differ only in their exponents and, therefore, commute. We find that it is never worse and often better to apply the  $U$ s in decreasing powers of two. This is because the sequence generated by  $U^{2^i} = x^{2^i} \bmod N$ ,  $i \geq 0$ , will eventually lead to a cyclic subsequence. Applying the  $U$ s in increasing powers saturates the rank in the fewest number of steps, which occurs just before the cycle repeats. In contrast, applying the  $U$ s in decreasing powers leads to performing the same operations on  $R$  at the beginning. Repeated operations will tend to populate the same states in  $R$  as previous applications, thus leads to a slower increase in ranks. Other orderings are also possible, but we have not considered them due to foresight of the forthcoming QFT. The rank between the rightmost control qubit and  $R$  reaches  $r$  once all unique  $U$ s have been applied.

Table I shows the ranks after each controlled- $U$  operation is applied, for the example  $N = 64$ ,  $x = 2$ , and  $r = 12$ . Time flows down the table, reflecting applying the  $U$ s in increasing powers of two. Our implementation places the most recently interacted control qubit furthest to the right, which leads to ordered qubits upon completing the controlled- $U$  gate sequence:  $q_0, q_1, \dots, q_{13}$ . Using this ordering, the state can be stored using 3300 complex numbers, or approximately 50KB. Table II shows the same simulation parameters, now with  $U$ s applied in decreasing powers, and hence reverse ordered qubits. Under this ordering, the same state can be stored using only 520 complex numbers, or approximately 8KB.

### B. Measurement of Lower Register

Measurement of the lower register requires the probability of each state  $i$  in  $R$ , which can be calculated from first principles using Eqn 5. One can show that this is

$$\text{pr}(i) = |\alpha_{ab\dots i}|^2 = R_i^\dagger \left\{ \dots \left[ \sum_b B_b^\dagger \left( \sum_a A_a^\dagger A_a \right) B_b \right] \dots \right\} R_i. \quad (9)$$

It is possible to enforce  $\sum_a A_a^\dagger A_a = 1$  for all qubits and qudits in the MPS by using the SVD exclusively. This allows one to calculate the probability of a given state of any qubit or qudit by using its own matrices only. However, this is not true in our simulations; we have sacrificed



measurement speed for simpler decompositions, namely Eqn 8.

Having computed the probabilities, one can apply a projection and rescale the remaining amplitudes. Since the projection will reduce the entanglement in the entire system, one should take this opportunity to reduce the space consumption. We apply the RRQRF pairwise from right to left for this purpose. We have chosen the RRQRF only for its rank-revealing property and its speed over the SVD, and not for any structure in the results. We have also avoided the faster LU decomposition as it is considered less numerically stable.

### C. The Quantum Fourier Transform

The typical circuit for the QFT is shown in Fig 2. The use of long-range controlled-phase gates make this circuit less than ideal when using a MPS simulator. Note that the final swap gates can be implemented classically and thus do not pose a problem.

To overcome this, one can be rearrange the QFT into  $2l$  subcircuits, each of which includes exactly one more qubit than its predecessor, as shown in Fig 3. One contracts a single qubit into a growing qudit at the beginning of each subcircuit, and applies all gates in the subcircuit directly onto this qudit. This arrangement is preferable because one eliminates the need to perform any matrix decompositions. Upon completion, a single  $2^{2l}$ -dimensional qudit remains (i.e. a  $2l$  qubit amplitude formalism state vector).

Another approach is to add swap gates after each controlled-phase gate, akin to implementing the QFT on a 1d quantum computer with only nearest neighbour interactions, as shown in Fig 4. This approach is initially slower, however, it may lead to better space performance when coupled to the SVD due to truncation of insignificant eigenvalues.

### D. Benchmarks

Table III shows the CPU times in seconds to simulate Shor's algorithm for various  $N$  and  $r$  for each of the described stages in the algorithm:  $t_U$  to apply all controlled- $U$  gates,  $t_{\text{meas}}$  to measure the lower register and minimise the ranks, and  $t_{\text{QFT}}$  to apply the QFT (using Fig 3). As the memory and time depends heavily on  $r$ ,  $x$  has been chosen ahead of time to maximise  $r$  for the given  $N$ , and we have also chosen cases where  $r \approx N/2$ . All simulations use a single core and double precision complex numbers; the  $l = 12$  case would require 1TB RAM on an amplitude formalism state vector simulator. The  $l \leq 12$  cases take minutes to run on a laptop (Intel Core 2 Duo P8400 @ 2.26GHz, 2GB RAM), and the  $l \geq 13$  cases take hours on a cluster (AMD Opteron @ 2.5GHz, 32GB RAM). For comparison,  $l = 12$  cases take 970s (IBM Regatta p690+, 512 processes) and 170s

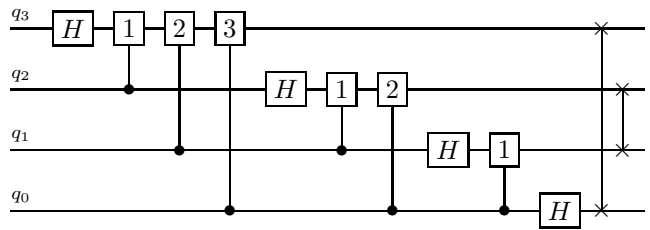


FIG. 2. Standard circuit implementing the quantum Fourier transform on four qubits. Controlled-phase gates performing  $|11\rangle \rightarrow \exp(i\pi/2^n)|11\rangle$  are denoted by the number  $n$  in a square. Swap gates are denoted by two crosses joined together by a vertical line. Long-range gates make this circuit less than ideal on a MPS simulator.

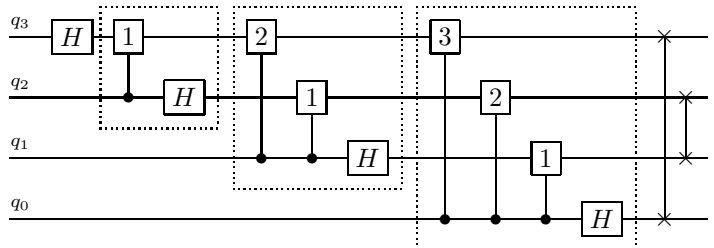


FIG. 3. QFT rearranged to be more compatible with MPS. Dashed boxes show the repetitive pattern of the subcircuits. No matrix decompositions are required, and all qubits involved are contracted into a single qudit at the completion of the circuit.

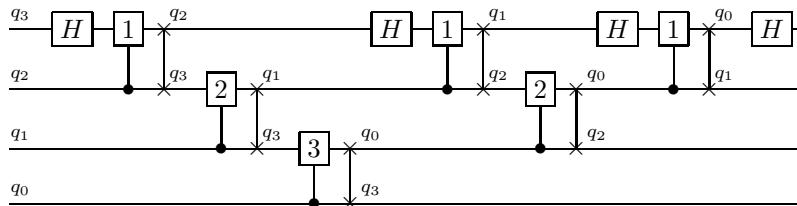


FIG. 4. QFT for a 1d nearest-neighbour quantum computer is also suitable for MPS. Matrix decompositions are only required after every swap operation.

(IBM BlueGene/L, 4096 processes) on very highly parallelised amplitude formalism simulators [7], corresponding to days in CPU time. The same software has been used to simulate  $l = 14$  cases, or equivalently 42 qubits (64TB RAM) [8].

## VI. MULTI-PROCESSOR IMPLEMENTATION

Simulations of Shor's algorithm benefit immensely from storing the state as a MPS. However, single process simulations will ultimately be memory limited, which is typically resolved by distributed computing. We show that MPS is well suited to this regime. We use the Message Passing Interface (MPI) [16] to manage inter-

$l$	11	12	13	14
$N$	2033	4063	8189	16351
	$(19 \times 107)$	$(17 \times 239)$	$(19 \times 431)$	$(83 \times 197)$
$x$	2	3	10	2
$r$	954	1904	3870	8036
$t_U$	0.2	0.1	2.6	3.8
$t_{\text{meas}}$	49	76	4843	12,799
$t_{\text{QFT}}$	11	6.7	962	1949
$t_{\text{total}}$	60	83	5808	14,752

TABLE III. CPU time in seconds the distinct steps of the order-finding circuit (Fig 1):  $t_U$  to complete all controlled- $U$ s;  $t_{\text{meas}}$  to measure out the lower register; and,  $t_{\text{QFT}}$  perform the QFT.  $t_{\text{total}}$  is the total time.  $x$  is chosen to maximise the order  $r$  for the given  $N$ .  $r$  determines the maximum size of the matrices before the QFT.

process communication, the PBLAS library [17] for basic distributed matrix operations, and ScaLAPACK [18] for linear algebra.

We assume that our processes are arranged into a 2d grid. For simplicity, we shall also assume that the number of processes  $n_{\text{proc}}$  is a power of two. The matrices associated with the qudits are divided and distributed to these processes. For our simulations, we have chosen to divide matrices into  $16 \times 16$  blocks, which are distributed cyclically. It is straightforward to port the program to this environment; many-qudit operations under MPS are simply some combination of matrix multiplications, re-arranging or adding sub-matrices, and matrix decomposition.

The simple data distribution described above works well for the majority of the simulation as the matrices are large and relatively square (Table I). However, one must take care during the QFT (Fig 3). This is because the circuit combines many qubits to form a very high dimensional qudit, with the most extreme case appearing upon completion, a single  $2^{2l}$ -dimensional qudit. One can easily produce unevenly distributed data, for example, by creating either  $2^{2l} 1 \times 1$  matrices (all data stored in a single process), or a single  $2^{2l}$ -dimensional row or column vector (data distributed along a single row or column only). To ensure a balanced data distribution throughout the circuit, we set the matrix's origin (i.e. the process containing the first element) to be the process whose rank is equal to the first  $\log_2(n_{\text{proc}})$  bits of the state. This is analogous to the distribution mechanic of large amplitude formalism simulators, where the most significant  $\log_2(n_{\text{proc}})$  bits of the state determine the process in which it is stored.

We have further divided the matrices into two aligned matrices, for the cases where the most significant qubit is  $|0\rangle$  and  $|1\rangle$ . Since the most significant qubit is the qubit to which the  $H$  gate is applied in each of the subcircuits in Fig 3, this allows  $H$  to be applied locally. Note that,

$l$	$N$	$n_{\text{proc}}$	$t_U$	$t_{\text{meas}}$	$t_{\text{QFT}}$	$t_{\text{total}}$
13	8189	1	3.4	6763	1539	8305
		2	2.1	3378	511	3891
		4	1.3	1636	253	1890
		8	0.7	886	128	1015
		16	0.5	452	76	529
14	16,351	1	6.3	13,173	3909	17,088
		2	3.6	5588	1430	7022
		4	1.8	2769	788	3558
		8	1.2	1471	356	1829
		16	0.7	741	172	914
15	32,663	4	5.2	7510	1934	9449
		8	3.1	3239	788	4031

TABLE IV. Wall-clock time in seconds for the distinct steps of the order-finding circuit for three cases:  $l = 13$ ,  $N = 8189 = 19 \times 431$ ,  $x = 10$ ,  $r = 3870$ ;  $l = 14$ ,  $N = 16351 = 83 \times 197$ ,  $x = 2$ ,  $r = 8036$ ; and,  $l = 15$ ,  $N = 32663 = 89 \times 367$ ,  $x = 6$ ,  $r = 16104$ .  $n_{\text{proc}}$  is the number of MPI processes or CPU cores.

as is the case for the amplitude formalism, the controlled-phase gates can also be applied without additional data transfer.

Table IV shows the wall-clock times in seconds for our implementation. These were run on the same cluster mentioned in the single process simulations (AMD Opteron @ 2.5GHz). The largest case simulated was  $l = 15$ , using approximately 16GB RAM spread over 8 processes and taking approximately one hour. Because these simulations were run on a shared cluster, the execution time can deviate by 25% or more, depending on the load on the nodes and the assignment of nodes. Thus the listed times are the lowest from each case, obtained from a small number of runs. The results indicate good scaling behaviour, doubling the number of processes leads to a 40-60% decrease in the total execution time.

We also mention here that there is another difference between these simulations and those of Table III. Recall that after the measurement projection, we apply a rank-revealing decomposition across the MPS to reduce the matrix sizes. Unfortunately, the QR decomposition from ScaLAPACK 1.8.0 (pzgeqpf) appears to *not* always choose pivots such that the diagonal (leading) elements of  $R$  are in order of descending magnitude, as described in [18]. This appears to be a bug, and the behaviour means we are unable to determine the numerical rank through this routine. Thus in these benchmarks, we have instead opted to use the SVD (pzgesvd).

## VII. CONCLUSION

We have shown that, in order to factorise an  $l$ -bit number  $N$  with order  $r$ , a MPS approach reduces the space complexity from  $O(2^{3l})$  to  $O(\max(4lr^2, 2^{2l}))$  in the case of dense storage. This is a significant improvement as  $r$  is typically much smaller than  $N$ , allowing one to simulate circuits with as many as 36 qubits on a standard laptops. Our largest simulation on a single processor of 42 qubits required less than 32GB RAM.

We have also ported our simulations to use MPI. We have simulated circuits with as many as 45 qubits over 8 CPU cores. Since MPS is built around matrix products, the distributed matrix approach to parallelisation understandably works well. Our benchmarks show near

$1/n_{\text{proc}}$  scaling.

One can extend these simulations, for example, by implementing the circuits for the controlled-unitaries, and by incorporating decoherence. Other quantum circuits with the same structure as the order-finding circuit are likely to benefit from an MPS approach, and many of the optimisations described here would be applicable to these and other MPS simulations.

This research was conducted by the Australian Research Council Centre of Excellence for Quantum Computation and Communication Technology (project number CE110001027). This research was supported in part by the U.S. Army Research Office (W911NF-08-1-0527), the US National Security Agency and the Albert Shimmins Memorial Fund.

- 
- [1] M. A. Nielsen, I. L. Chuang, Quantum computation and quantum information, Cambridge University Press, Cambridge, 2000.
  - [2] P. W. Shor, Algorithms for quantum computation: discrete logarithms and factoring, in: Proc. 35th Annu. Symp. Found. of Comput. Sci., 1994, pp. 124–134.
  - [3] P. W. Shor, Polynomial-time algorithms for prime factorization and discrete logarithms on a quantum computer, SIAM J. Comput. 26 (1997) 1484–1509.
  - [4] K. M. Obenland, A. M. Despain, A parallel quantum computer simulator, presented at High Performance Computing 1998.
  - [5] J. Niwa, K. Matsumoto, H. Imai, General-purpose parallel simulator for quantum computing, Phys. Rev. A 66 (2002) 062317.
  - [6] F. Tabakin, B. Juliá-Díaz, Qcmpi: a parallel environment for quantum computing, Comput. Phys. Commun. 180 (2009) 948–964.
  - [7] K. D. Raedt, K. Michielsen, H. D. Raedt, B. Trieu, G. Arnold, M. Richter, T. Lippert, H. Watanabe, N. Ito, Massive parallel quantum computer simulator, Comput. Phys. Commun. 176 (2007) 121–136.
  - [8] Helmholtz Association of German Research Centres, World record: Jülich supercomputer simulates quantum computer, Press release, retrieved from <http://www2.fz-juelich.de/portal/index.php?cmd=show&index=163&mid=761> (2010).
  - [9] G. Vidal, Efficient classical simulation of slightly entangled quantum computations, Phys. Rev. Lett. 91 (2003) 147902–147905.
  - [10] D. Coppersmith, An approximate Fourier transform useful in quantum factoring, Tech. Rep. RC 19642, T. J. Watson Research Center, IBM Corporation (1994).
  - [11] C. Zalka, Fast versions of Shor’s quantum factoring algorithm, quant-ph/9806084.
  - [12] S. Beauregard, Circuit for Shor’s algorithm using  $2n+3$  qubits, Quantum Inf. Comput. 3 (2003) 175–185.
  - [13] D. E. Browne, Efficient classical simulation of the quantum Fourier transform, New J. Phys. 9 (2007) 146.
  - [14] N. Yoran, A. J. Short, Classical simulability and the significance of modular exponentiation in Shor’s algorithm, Phys. Rev. A 76 (2007) 060302(R).
  - [15] R. Jozsa, N. Linden, On the role of entanglement in quantum-computational speed-up, Proc. Roy. Soc. Lond. A 459 (2003) 2011–2032.
  - [16] Message passing interface forum, <http://www.mpi-forum.org/>.
  - [17] Parallel BLAS, [http://www.netlib.org/scalapack/pblas\\_qref.html](http://www.netlib.org/scalapack/pblas_qref.html).
  - [18] L. S. Blackford, J. Choi, A. Cleary, E. D’Azevedo, J. Demmel, I. Dhillon, J. Dongarra, S. Hammarling, G. Henry, A. Petitet, K. Stanley, D. Walker, R. C. Whaley, ScaLAPACK Users’ Guide, Society for Industrial and Applied Mathematics, Philadelphia, PA, 1997.